The Recombination Velocity at III-V Compound Heterojunctions with Applications to $Al_xGa_{1-x}As$-$GaAs_{1-y}Sb_y$ Solar Cells

論 文
28—4—3

金 正 淳*
(Jung-Soon Kim)

Abstract

Interface recombination velocity in Al_xGa_{1-x} As-$GaAs$ and $Al_{0.85}$ $Ga_{0.15}$ As-$GaAs_{1-y}Sb_y$ heterojunction systems is studied as a function of lattice mismatch. The results are applied to the design of highly efficient III-V heterojunction solar cells.

A horizontal liquid-phase epitaxial growth system was used to prepare p-p-p and p-p-n Al_xGa_{1-x} As-$GaAs_{1-y}Sb_y$-$Al_xGa_{1-x}As$ double heterojunction test samples with specified values of x and y. Samples were grown at each composition, with different GaAs and GaAs Sb layer thicknesses.

A method was developed to obtain the lattice mismatch and lattice constants in mixed single crystals grown on (100) and (111)B oriented GaAs substrates. In the AlGaAs system, elastic lattice deformation with effective Poisson ratios ν_{eff} (100=0.312 and ν_{eff} (111B) =0.190 was observed. The lattice constant a_0 $(Al_xGa_{1-x}As)=5.6532+0.0084x$ Å was obtained at 300K which is in good Agreement with Vegard's law. In the GaAsSb system, although elastic lattice deformation was observed in (111) B-oriented crystals, misfit dislocations reduced the Poisson ratio to zero in (100)-oriented samples. When a_0 $(GaSb)=6.0959$ Å was assumed at 300K, both (100) and (111)B oriented GaAsSb layers deviated only slightly from Vegard's law. Both (100) and (111)B zero-mismatch $Al_{0.85}$ $Ga_{0.15}$ As-$GaAs_{1-y}Sb_y$ layers were grown from melts with a weight ratio of $W_{Sb}/W_{Ga}=0.13$ and a growth temperature of 840 to 820°C. The corresponding Sb compositions were $y=0.015$ and 0.024 on (100) and (111)B orientations, respectively. This occurs because of a fortuitous variation in the Sb distribution coefficient with orientation.

Interface recombination velocity was estimated from the dependence of the effective minority carrier lifetime on double-heterojunction spacing, using either optical phase-shift or electroluminescence timedecay techniques. The recombination velocity at a (100) interface was reduced from (2 to 3)$\times 10^4$ for $y=0$ to (6 to 7)$\times 10^3$ cm/sec for lattice-matched $Al_{0.85}Ga_{0.15}As$-$GaAs_{0.985}Sb_{0.015}$ Although this reduction is slightly less than that expected from the exponential relationship between interface recombination velocity and lattice mismatch as found in the AlGaAs-GaAs system, solar cells constructed from such a combination of materials should have an excellent spectral response to photons with energies over the full range from 1.4 to 2.6 eV. Similar measurements on a (111) B oriented lattice-matched heterojunction produced some-what larger interface recombination velocities.

* 正會員 : 美國 Stanford University(工學博士)
接受日字 1979年 2月 13日

1. INTRODUCTION

Although theoretical studies [1,2] have demonstrated that GaAs should be one of the best materials for constructing solar cells, the efficiency of the early p-n junction GaAs solar cells was poor. The reasons for this inefficiency are that this direct band-gap material requires the p-n junction to be less than 1 μm from the surface and that the GaAs-air interface has a large surface recombination velocity of approximately 10^6 cm/sec.

These difficulties were overcome during the early 1970's by growing thin (p) $Al_xGa_{1-x}As$ layers on the surfaces of p-n junction GaAs solar cells. Although this window layer is opaque to high-energy photons (>2.0 eV), the heterojunction confines the photon-generated electrons with in the (p) GaAs layer, thereby providing a low-interface recombination velocity that greatly increases the efficiency compared to that of a simple GaAs cell; efficiencies up to 21 percent at AM1.4 have been reported [3].

Even after this improvement, efficiency was still far from the theoretical value (~27percent), perhaps as a result, in part, of lattice mismatch at the heterojunction interface. The lattice constant a_0 of GaAs, AlAs, and GaSb single crystals at room temperature is 5.6532, 5.6622, and 6.0959 Å, respectively [4]. The mismatch at a GaAs-AlAs heterojunction is thus 0.16 percent and, if Vegard's law is obeyed, the mismatch at a $GaAs\text{-}Al_xGa_{1-x}As$ heterojunction is 0.16x percent. This mismatchis small in comparison to other known heterojunction systems; however, it is large enough to produce finite interface recombination velocities. The fact that this lattice mismatch can be eliminated by adding Sb to GaAs led to the measurement of recombination velocity at a lattice-matched AlGaAs-GaAsSb interfaceas well as at $Al_xGa_{1-x}As\text{-}GaAs$ interfaces. Electroluminescent time-decay and optical phase-shift techniques were employed to determine the heterojunction-interface recombination velocities, and a double-crystal X-ray diffractometer was used to measure precise heterojunction lattice mismatch. Based on these data $Al_xGa_{1-x}As\text{-}GaAs_{1-y}Sb_y$ solar cells can be optimized to achieve maximum efficiency.

Methods to obtain the interface recombination velocity are theoretically analyzed in Chapter II, and relevant sample structures and techniques for measuring effective lifetimes are discussed. Liquid phase epitaxial (LPE) growth techniques, including melt and substrate preparation and procedures for growing double-heterojunction (DH) samples, are described in Chapter III, followed by characterization of the grown lay ers. In Chapter IV, theoretical relations are derived to determine both strained and strain-free lattice mismatch between the epitaxial layer and the substrate, assuming only two simplified lattice defects (elastic lattice deformation and misfit dislocations). Experimental results from AlGaAs-GaAs and GaAsSb-GaAs interfaces are described in detail. Schematics of the apparatus employed to evaluate effective lifetimes using both optical phase-shift and electroluminescent (EL) time-decay measurement techniques are presented in Chapter V. Interface recombination velocities are evaluated from best-curve fits based on heterojunction spacing and measured effective lifetime for fixed bulk lifetime and minority carrier diffusion length. Recombination velocities, $S=(2\text{ to }3)\times10^4$ and $(6\text{ to }7)\times10^3$ cm/sec, were achieved at ($\bar{1}00$) $Al_{0.85}Ga_{0.15}As\text{-}GaAs$ and lattice-matched $Al_{0.85}Ga_{0.15}As\text{-}GaAs_{0.985}Sb_{.0015}$ heterojunction interfaces, respectively. A summary of the significant aspects of this research and suggestions for future study are included in Chapter VI.

2. INTERFACE RECOMBINATION VELOCITY

Interface recombination velocity can be determined from the dependence of the minority carrier lifetime on heterojunction spacing of symmetrical double-heterostructure (DH) samples. This is analogous to a semiconductor slab conf-

ined by two surfaces of equal recombination velociy [5,6,7].

A. Theory

A symmetrical $Al_xGa_{1-x}As$-$GaAs_{1-y}Sb_y$ DH sample is illustrated in Fig. 1. where Al comptosition x and recombination velocity S are assumed to be the same at both heterojunctions. It is also assumed that (1) the sample is an infinite slab of extrinsic p-type, (2) external surface excitation is uniform throughout the illuminated heterojunction interface, and (3) the electron-hole pairs are generated only near the interface. This is true when the sample is excited by laser light which has a photon energy larger than the band gap of the $GaAs_{1-y}Sb_y$ layer and smaller than that of the $Al_xGa_{1-x}As$ layer. In addition, low-level excitation assumed so that the injected minority carrier (electron, in this case) density Δn is much less than the background hole density. Possible effects caused by light reabsorption with in the recombination region are neglected in this analysis.

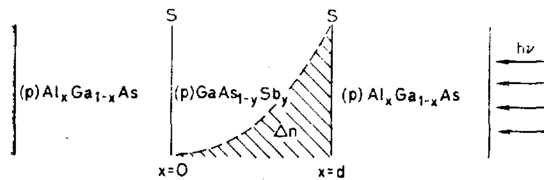

Fig. 1 One-dimensional diagram of a Symmetrical (p) AlGaAs-(p) GaAsSb DH Infinite Slab.

The continuity equation of minority carriers for the steady-state case and the relations for the two boundary conditions at the interface are

$$D_n(d^2\Delta n/dx^2)-\Delta u/\tau_0=0 \quad (2.1)$$

and

$$-D_n(d\Delta n/dx)_{x=d}+G_s=S(\Delta n)_{x=d} \quad (2.2a)$$

$$D_n(d\Delta n/dx)_{x=0}=S(\Delta n)_{x=0} \quad (2.2b)$$

where D_n is the diffusion constant of the minority carriers and τ_0 is the bulk lifetime in the p-type semiconductor. These quantities are related to the bulk-electron diffusion length by $L_n=(D_n\tau_0)^{1/2}$. The generation rate G_s is included in the boundary condition [Eq. (2.2a)] rather than in the continuity equation, for simplicity. In this analysis trapping was not considered.

From the solution of Eq. (2.1), the excess minority carrier density is [5,6]

$$\Delta n(x)=G_s/d)(d/2L_n)^2\times\frac{(d/L_n)\cosh(x/L_n)}{\{(Sd/2D_n)^2+(d/2L_n)^2\}}$$
$$\frac{+(Sd/D_n)\sinh(x/L_n)}{\sinh(d/L_n)+(Sd/2D_n)(d/L_n)\cosh(d/L_n)} \quad (2.3)$$

With the following definitions,

$$\Delta\bar{n}=(1/d)\int_0^d n(x)dx=(G_s/d)\ \tau_{eff}$$

$$\xi=SL_n/D_n$$

Eq. (2.3) can be simplified to

$$(\tau_{eff}/\tau_0)=\frac{\sinh(d/L_n)+(\cosh(d/L_n)-1)}{(\xi^2+1)\sinh(d/L_n)+2\xi\cosh(d/L_n)} \quad (2.4)$$

where

$\Delta\bar{n}$=average injected minority carrier density

τ_{eff}=effective minority carrier lifetime

ξ=normalized interface recombination velocity

When $d\ll L_n$ and $\xi\ll 1$, Eq. (2.4) reduces to $(1/\tau_{eff})=(1/\tau_0)+(2S/d)$. Figure 2 is a plot of the normalized effective minority carrier lifetime τ_{eff}/τ_0 as a function of the normalized heterojunction spacing d/L_n for various values of ξ.

Figure 2 implies that, if τ_0 and L_n are known, the interface recombination velocity can be determined by curve fitting [8,9] from the measurement of the effective minority carrier lifetime and heterojunction spacing. It also shows a reduction of τ_{eff} with decreasing values of d.

B. Measuring Techniques

As discussed above, when τ_0 and L_n are known, the interface recombination velocity can be obtained from the dependence of effective minority carrier lifetime on the heterojunction spacing of symmetrical DH samples. The next problem is to select measuring techniques that are available and feasible among the existing instruments for determining effective minority carrier lifetimes.

Several available techniques include electroluminescent(EL) time decay [6,7,8], pulsed reverse-bias recovery [10,11], current decay from pulsed laser beams [12], and optical phase shift [13,

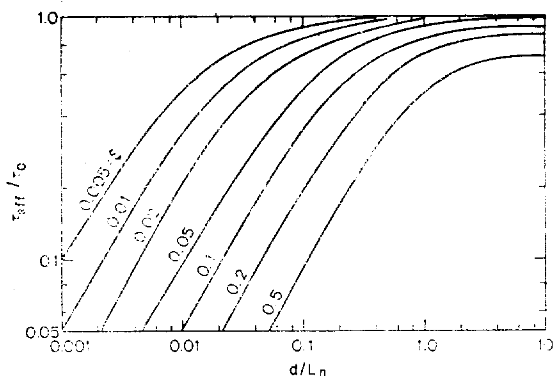

Fig. 2 Normalized Effective Minority Carrier Lifetime (τ_{eff}/τ_0) as a Function of Hheterojunction Spacing (d/L_n) The independent parameter is the interface recombination velocity ξ.

14]. Among these, EL time-decay and optical phase-shift techniques were chosen, and the p-p-p and p-p-n DH samples were used for the optical and EL measurements respectively. Effective minority carrier lifetime can be directly deter mined from EL time-decay measurements but only indirectly from optical phase-shift measurements (see Chapter V for additional details). The heterojunction spacing d was determined with a conventional optical microscope after staining the cleaved edges of the samples.

C. Sample Structure

Figure 3 presents energy-band diagrams of the test samples. Figure 3a is the energy-band diagram of a p-p-p DH sample, and Figs. 3b and 3c apply to unbiased and biased p-p-n DH diodes. A similarity can be observed between(a) and (c), especially in the p-p-n DH diodes when the (p) GaAs [or (p) GaAsSb] layers were more heavily doped than the (n) AlGAAS layers. In this case, it can be assumed that the depletion region (approximately 0.1 μm in thickness) at the p-n junction is located inside the (n) AlGaAs layer and that the electron-hole pair recombination rate caused by space charge is thus minimized.

DH samples with various heterojunction spacings (0 to 15 μm) were prepared by liquid phase epitaxial (LPE) growth techniques on the GaAs substrates. Details regarding LPE crystal growth are discussed in Chapter III. In this study, the

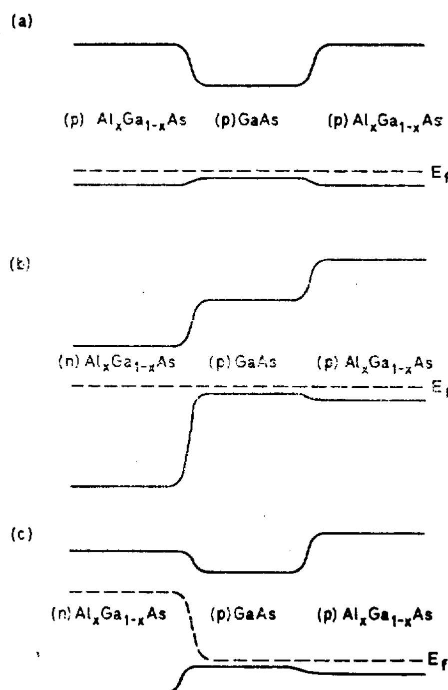

Fig. 3 Energy-band Diagrams of DH dhsamples. (a) p-p-p DH Sample, (b) p-p-n DH diode under no bias, and (c) p-p-n DH diode under forward bias.

Al composition x of the $Al_xGa_{1-x}As$ layers was set at x=0.85. The corresponding band-gap energy is ~2.05 eV Although attempts were made to grow $Al_xGa_{1-x}As$ layers with $x \approx 1$ so as to increase the spectral response of the solar cells at shorter wavelengths, the surface morphology of the higher Al composition AlGaAs layers degraded in a short time. Both $Al_{0.85}Ga_{0.15}As$-$GaAs$ and latticematched $Al_{0.85}Ga_{0.15}As$-$GaAs_{1-y}Sb_y$ DH samples were prepared for evaluation.

3. LIQUID PHASE EPITAXIAL GROWTH

A. Growth Technique

The growth conditions have been determined for preparing $Al_xGa_{1-x}As$ and $GaAs_{1-y}Sb_y$ single crystals with specified values of x and y. These values were controlled by adding known amounts of Al or Sb to As-saturated Ga melts. Figure 4 is a diagram of the horizontal sliding-boat LPE

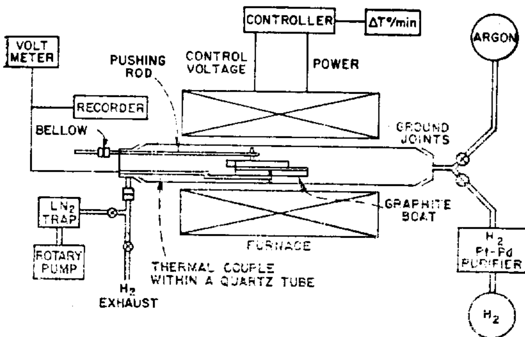

Fig. 4. Horizontal Sliding boat LPE Growth System.

growth system (vacuum tight) used in this study and described in detail by Cheung [15]. The samples were grown in flowing H_2 at atmospheric pressure. The growth temperature was 850° to 820°C, and the cooling rate was 0.2 or 0.4° C/min. All p-type layers were doped with Ge(p= 2 to $5\times10^{17}/cm^3$ in GaAs and GaAsSb and $\approx1\times10^{18}/cm^3$ in AlGaAs) [16, 17, 18]. All n-type layers were doped with Sn ($n\lesssim10^{17}/cm^3$2in AlGaAs [16, 19].

1. Melt and Substrate Preparation

The GaAs, AlGaAs, and GaAsSb layers were grown by LPE in the Ga-rich corner of the ternary phase diagram. Six 9's pure Ga melts were first baked out in flowing H_2 at 800°C for 12 hours to remove volatile contaminants such as oxygen, and then an undoped polycrystalline GaAs wafer, pure Al, pure Sb, and dopants were added as required.

To ensure melt saturation and to reduce oxide contamination, an undoped GaAs wafer, larger than actually required to saturate the melt at the growth temperature, was placed on the top of each melt. Either Te-or Cr-doped (100) and/or (111)B GaAs substrates (14 mils thick) were loaded in the recess adjoining the melts. The Te-doped GaAs substrate had a carrier concentration of approximately $n=2\times10^{18}/cm^3$

Before loading into the system, all the materials were successively degreased by trichloroethylene, acetone, and methanol in an ultrasonic bath and then soaked in HCl for three minutes to remove surface oxide. Following this procedure, special care was taken to avoid exposing the materials to air. They were thoroughly rinsed in methanol several times by dilution the HCl solution with methanol and then in hot electronic-grade isopropyl-alcohol and blown dry using filtered N_2 before loading. During preparation, the substrates were held by an especially designed quartz tweezer to avoid surface damage during the cleaning process

2. Growth Procedure

Previous growth techniques were modified[15, 20] to improve the surface morphology of as-grown multiple layers by reducing the lateral spacing between the GaAs and the AlGaAs melts. This reduction lessens the time when the substrate is exposed to the H_2 flow during transfer from one melt to the next. Growth procedures for p-p-p and p-p-n DH samples will be described using the diagram of the graphite boat in Fig. 5. After loading, the system was purged with H_2, pumped to less than 1 Toor, and then backfilled with H_2 at a flow rate of 120cc/min.

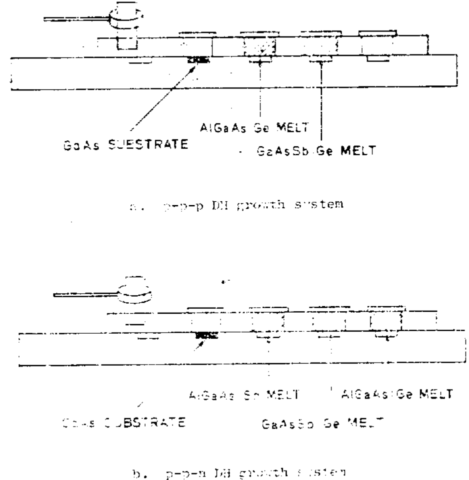

Fig. 5. Sliding Graphite-boat Growth System.

Inthe p-p-p DH growth,AlGaAs and GaAs (or GaAsSb) melts were prepared, and the GaAs substrate was loaded in the recess next to the AlGaAs melt. After the temperature controller was turned on at the initial growth temperature (0.4° C/min cooling rate), the top plate was pulled from the starting position to the left to grow the

first AlGaAs layer, pulled to the left a second time to grow the GaAs (or GaAsSb) layer, moved to the right to grow the second AlGaAs, and then was returned to the starting position.

In the p-p-n DH growth, two AlGaAs (one Sn-doped, and the other Ge-doped) and one GaAs (or GaAsSb) melts were prepared. The procedure was similar to the p-p-p DH growth except that the top plate was pulled successively to the left to grow the three layers, after which the furnace was removed and the inlet and outlet valves were closed. When room temperature was reached, the system was returned to its starting position by moving the top plate to the right. The reason for this last procedune is to intentionally grow a thin GaAs layer on the top of the second AlGaAs layer because Al in the grown layer depletes during the cooling process An ohmic contact to this GaAs layer is esaily made.

B. Solidus Composition of Grown Layers

Solidus compositions of the grown AlGaAs and GaAsSb layers were determined by standard electron-microprobe analyses. Both (100)- and (111) B-oriented GaAs substrates were used. Thicknesses of the epitaxial layers were several micrometers, and the accelerating voltage in the electron microprobe was 10 keV.

1. Al Composition

Figure 6 plots the solidus Al composition in $Al_xGa_{1-x}As$ single layers as a function of the weight ratio W_{Al}/W_{Ga} in the melt. For example, crystals with x=0.85 were grown at 840°C, using an Al/Ga weight ratio of 9.8×10^{-3} in the As saturated melt.

Two sets of samples were grown at different temperature ranges. Higher Al compositions were obtained at the lower growth temperature for a given weight ratio because of a higher distribution coefficient of Al at the lower temperature (see Table 1). In addition, the Al distribution coefficient, at a fixed growth temperature, increased when the Al/Ga weight ratio in the melt decreased. The same Al composition was obtaine on both (100)-and (111)B-oriented GaAs substrates when grown simultaneously from the same melt.

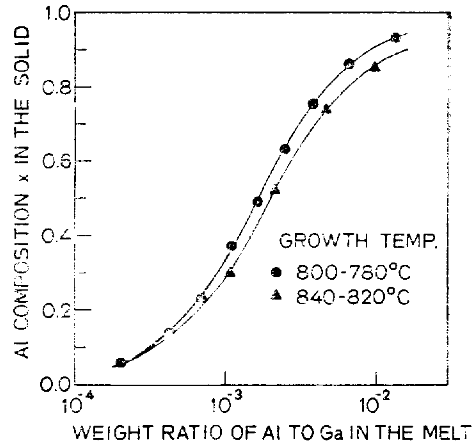

Fig. 6. Solidus al composition in LPE AlGaAs layers vs weight ratio of al to Ga in the melt. Two growth temperature ranges are shown.

Table 1 GRrowth data of LPE AlGaAs Single layers

Sample No.	Melt Weight Ratio $W_{Al}/W_{Ga}(\times10^{-3})$	Al Composition x	Al Distribution Coefficient D+
T_G=840 to 820°C			
201B	1.057	0.299	109.5
201A	2.199	0.520	91.55
152X	4.665	0.738	60.99
140Y	9.731	0.851	33.39
T_G=800 to 780°C			
113J	0.202	0.06	115.2
114J	0.426	0.14	127.3
115J	0.689	0.23	129.2
116J	1.087	0.37	131.7
117J	1.629	0.49	116.4
118J	2.481	0.63	98.3
119J	3.762	0.75	77.2
120J	6.579	0.86	50.6
121J	13.390	0.93	26.9

+D is the ratio of the atomic fraction of the substituting element in the crystalline solid to that in the liquid melt.

This impslie that the distribution coefficient of Al is independent of substrate orientation.

2. Sb Composition

Figure 7 plots the solidus Sb composition in $GaAs_{1-y}Sb_y$ single layers as a function of the

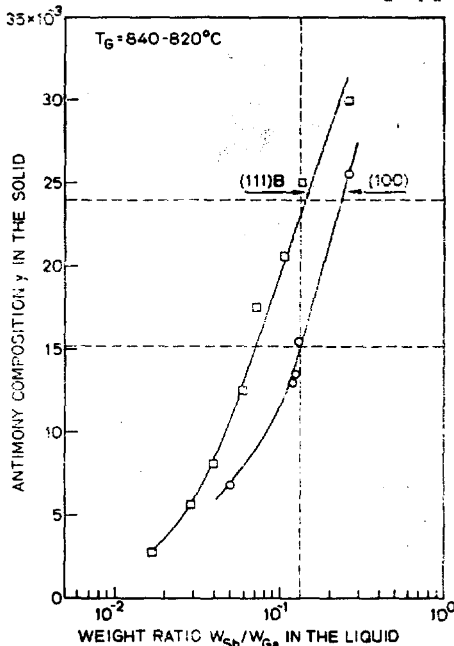

Fig. 7. **Solidus Sb composition in LPE $GaAs_{1-y}Sb_y$ layers VS weight ratio of Sb To Ga in the melt. Results on (100)-and (111)B-oriented Ga Assubstrates are shown.**

weight ratio W_{Sb}/W_{Ga} in the melt at a growth temperature of 840 to 820°C. The antimony composition varied from $y=0$ to $y=0.03$. Detailed growth information is listed in Table 2. Data points are somewhat scattered because of uncertainty in the Sb compositions. Antimony concentration profiles of very thick (30μm) GaAsSb single layers, along cleaved edges, indicated that Sb concentration is constant with depth.

When $GaAs_{1-y}Sb_y$ layers were grown simultaneously on both (100)-and (111)B-oriented GaAs substrates from the same melt, a higher Sb composition y was obtained on the (111)B substrate. For example, at a weight ratio of $W_{Sb}/W_{Ga}=0.13$, $y=0.015$ and 0.024 on the (100) and (111)B substrates, respectively. The corresponding Sb distribution coefficients are $D=0.21$ and 0.34. These observations reveal that Sb has a higher distribution coefficient on the (111)B-oriented substrates (see Table 2).

It can be seen in Figs. 6 and 7 that $Al_xGa_{1-x}As$-$GaAs_{1-y}Sb_y$ double-heterojunction samples can

Table 2. Growth data of LPE GaAsSb single layers

Sample No.	Melt Weight Ratio W_{Sb}/W_{Ga} ($\times10^{-2}$)	Sb Composition y	Sb Distribution Coefficient D
(100) Orientation			
203	0.0069	0.050	0.241
155X	0.0129	0.120	0.188
153	0.0133	0.125	0.186
206	0.0155	0.130	0.208
154X	0.0251	0.263	0.167
(111)B Orientation			
122Y	0.0027	0.017	0.277
125X	0.0056	0.028	0.349
123Y	0.0082	0.040	0.358
123X	0.0126	0.060	0.367
124X	0.0174	0.074	0.413
124Y	0.0206	0.101	0.356
205	0.0250	0.130	0.336
154Y	0.0300	0.263	0.199

be grown with a wide range of Al and Sb compositions.

C. Layer Characterization

Figure 8 is a series of photomicrographs of the surface morphology of undoped as-grown single layers (several μm in thickness). The first two layers (Figs. 8a and 8b) were grown on (100)-oriented GaAs substrates, and the second two layers (Figs. 8c and 8d) were grown on (111) B-oriented GaAs substrates. The surface morphology of the InGaAs layer was very poor, and the layer could be grown on only (111)B-oriented GaAs substrates[21, 22, 23, 24]. The surface morphology of the others was very good.

At the beginning stage of this research, InGaAs layers were grown to provide a zero mismatch with $Al_{0.85}Ga_{0.15}As$. This work was abandoned altshough the InGaAs layer had better solar-cell spectral response at long wavelengths [4, 25] than did the GaAsSb layers when lattice-matched with $Al_{0.85}Ga_{0.15}As$. Poor surface morphology of the InGaAs LPE layers grown in the Ga-rich corner of the ternary phase diagram was the result of inadequate wiping of the melt [26].

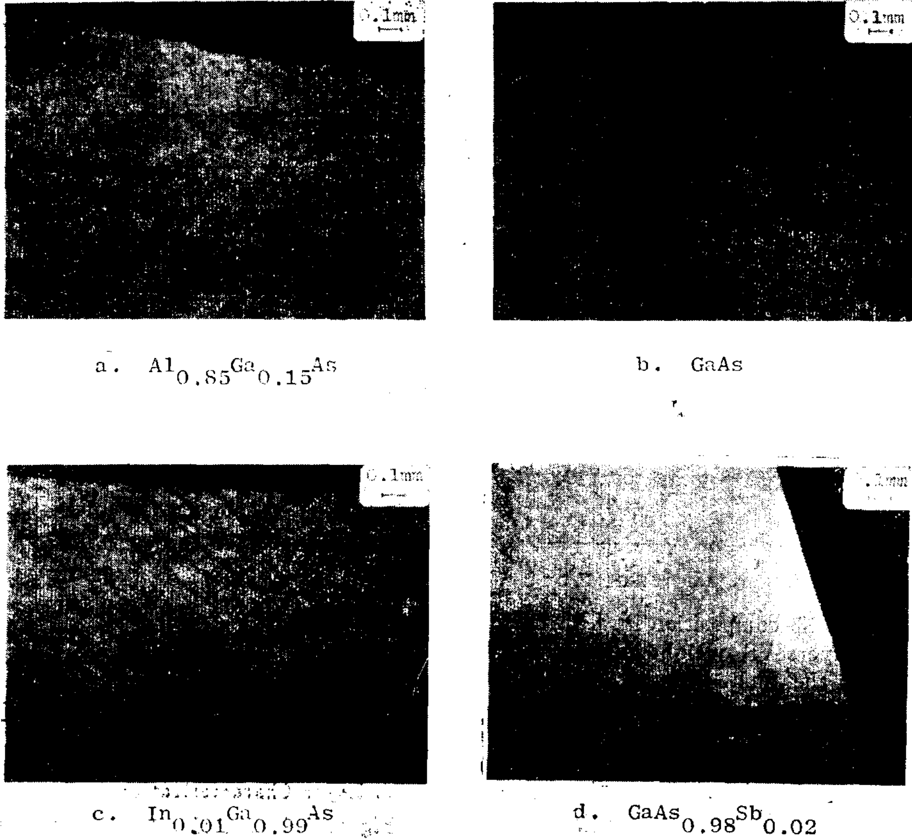

Fig. 8. Photomicrographs showing surface morphology of As-grown LPE single layers.

The surface morphology of the AlGaAs-InGaAs DH samples was even poorer.

Figure 9 shows the cross section of an $Al_{0.85}Ga_{0.15}As$-$GaAs$ DH sample and its Al line profile as recorded by the electron-microprobe analyzer. The sample was grown on a (100)-oriented GaAs: Te substrate and cleaved with a diamond scriber. The cleaved edge was stained in a PA solution (3 drops NH_4OH+200ml H_2O_2: PH=7) for 10 min and rinsed in methanol [27, 28]. It can be observed that all the interfaces are straight and parallel. The layer thicknesses, from left to right, are 5.0, 6.6, and 5.8μm, respectively.

The electron microprobe had a 10.0 KeV accelerating voltage, and the effective diameter of excitation at this voltage was approximately 6 μm. The line profile, which is a reproduction of the original recrding, was used to determine the Al composition x of the $Al_xGa_{1-x}As$ layers by standard microprobe analyses. A value of $x=0.85\pm0.01$ was obtained from the two layers.

Figure 10 is the PL spectra of the sample in Fig. 9 at room and LN_2 temperatures. A 6471 Å Kr-ion laser was used for excitation. The PL output is from the GaAs: Ge layer only. The band-gap energy of GaAs: Ge shifted from 1.4285 eV at 300K to 1.5083 eV at 77K. Although only one peak, caused by band-to-band transitions, was observed at 300K, two additional peaks are seen at 77K resulting from transitions from Ge impurity levels to the conduction band. The activation energies of these two acceptor levels are 28.5 and 68.7 meV [29, 30].

The sharp PL spectrum at 77K indicates that there was almost no Al concentration gradient

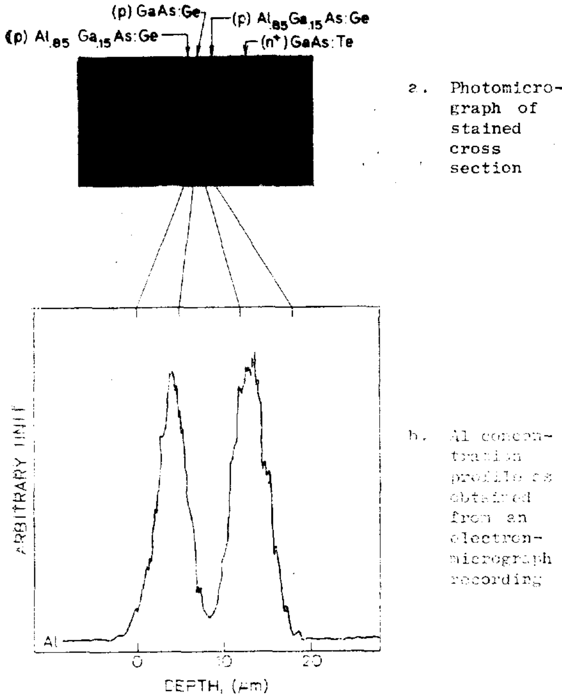

Fig. 9. An $Al_{0.85}Ga_{0.15}$ As:GaAs: Ge DH Sample.

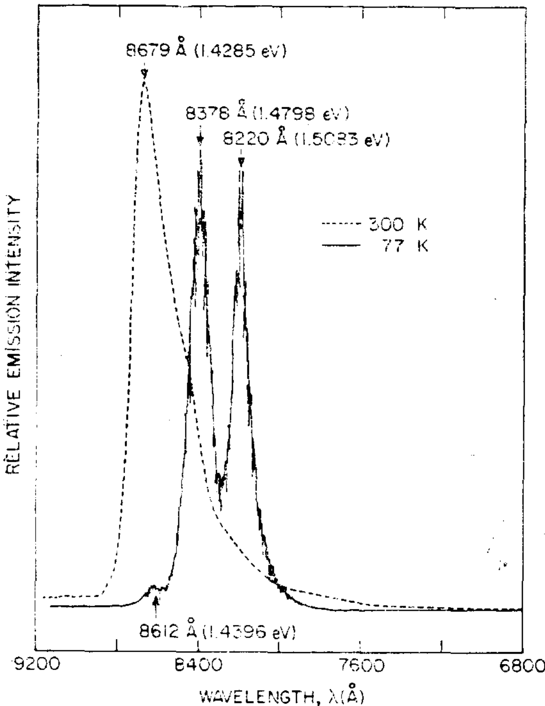

Fig. 10. Photoluminescent spectra of $Al_{0.85}Ga_{0.15}$ As: Ge-GaAs: Ge DH sample. A 6471 Å Kr laser was used for excitation, and the PL output came from the GaAs: Ge layer only.

at the heterojunction niterface. Precise measurements by Auger analysis revealed that the interface-transition width was approximately 210 Å (a nearly abrupt heterojunction) and that there was no detectable cross diffusion of Al (or Sb in the $Al_{0.85}Ga_{0.15}As$-$GaAs_{1-y}Sb_y$ DH samples) at the interface. Additional details of the Auger measurements have been reported [31,32].

Figure 11 is a cross section of the(100)-oriented $Al_{0.85}Ga_{0.15}As$-$GaAs_{0.985}Sb_{0.015}$ DH diode. Because no energy barrier for majority carriers existed, both p-p and n-n heterojunctions were ohmic. The substrate side of the as-grown sample was lapped to reduce the total thickness to less than 7 mils. The Au+12% Ge: Ni and Au+ 10% Zn alloys were evaporated onto the n-type substrate and the p-type GaAs layer, respectively, and were then alloyed at450°C for 5 min to form ohmic contacts. After they were cleaved into small pieces (usually less than $2\times1mm^2$), each diode was mounted on a TO-5 header.

Figure 12 shows the I-V characteristic curve and EL output of the above diode at 300K. In the I-V curve, a threshold voltage of approximately 0.9V and a breakdown voltage of 5V were obtained in the forwardand reverse-bias directions, respectively. It was observed that the breakdown voltage of GaAs (or GaAsSb) homojunction diodes was generally several times higher than that of the DH diodes. The EL output was obtained at a current density of 35 A/cm^2. At the low current-density level, the EL peak ($\lambda=$ 9195 Å) was located at a longer wavelength than was the PL peak (λ=8973Å) for the same amount of Sb ($y=0.015$), When the current density was increased. the EL peak moved to a shorter wavelength.

Figure 13 shows the arrangement used for measuring minority carrier diffusion length with a scanning electron microscope in the induced-current mode: semi-log plots of induced-current vs beam position are included. For additional details, see Refs. 20,33,and 34. A (100)-oriented $Al_{0.85}Ga_{0.15}As$-$GaAs_{0.985}Sb_{0.015}$ DH diode (see inset) was used to measure the diffusion lengths in both the (p)GaAsSb and (n) AlGaAs layers. The

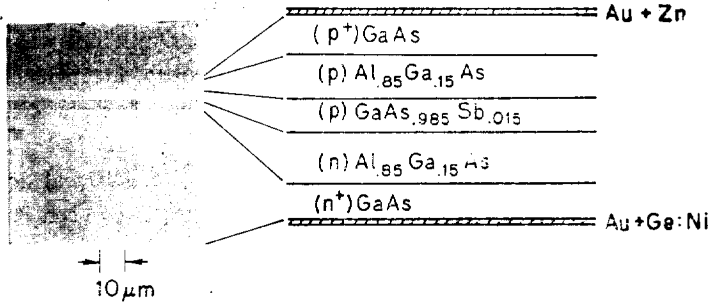

Fig. 11. Photomicrograph of stained cross section of a (100)-(oriented $Al_{0.85}Ga_{0.15}$ As-$GaAs_{0.985}Sb_{0.015}$ DH diode.

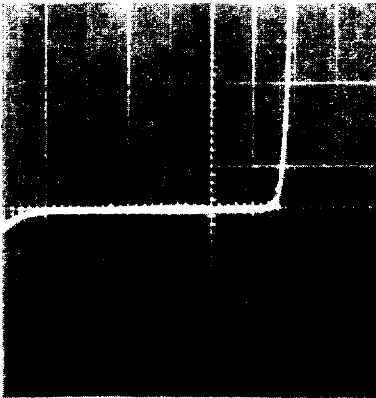

a. I-V characteristic curve

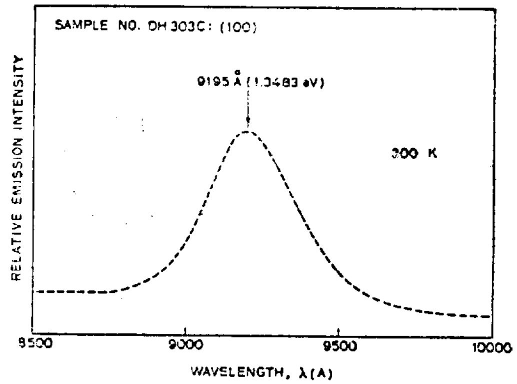

b. EL output

Fig. 12. (100)-Orien ted $Al_{0.85}Ga_{0.15}As$-$GaAs_{0.985}Sb_{0.015}$ DH diode.

corresponding carrier concentrations were (2 to 5)$\times 10^{17}/cm^3$ and $\lesssim 10^{17}/cm^3$, respectively. The electron beam energy for the measurements was 25 keV. The inset at the bottom of Fig. 13 is an induced-current trace superimposed on the secondary emission image, and the position of the p-n junction is identified from the peak of this trace. The minority carrier diffusion lengths obtained from the slopes of the straight-line regions in the semi-log plots were L_n ≒ 1.49 μm and $L_p = 0.73 \mu m$. The exceptionally short lengh of L_n [24] may be the result of the cross-hatched patterns always observed on (100)-oriented GaAsSb layers (see Fig. 14). The minority carrier diffusion lengths of Ge-doped GaAs layers were not measured in this study; instead, $L_n = 12 \mu m$ obtained by Ettenberg et al [6] was used in the evaluation of interface recombination velocity at an AlGaAs-GaAs interface as described in Chapter V-

Symbols

- a_f lattice constant of epitaxial layer (Å)
- $a^{\parallel}_f$ strained lattice constant of epitaxial layer parallel to substrate surface (Å)
- $a_f^{\perp}$ strained lattice constant of epitaxial layer perpendicular to substrate surface (Å)
- a_0 lattice constant (Å)
- a_s lattice constant of substrate (Å)
- C real quantity

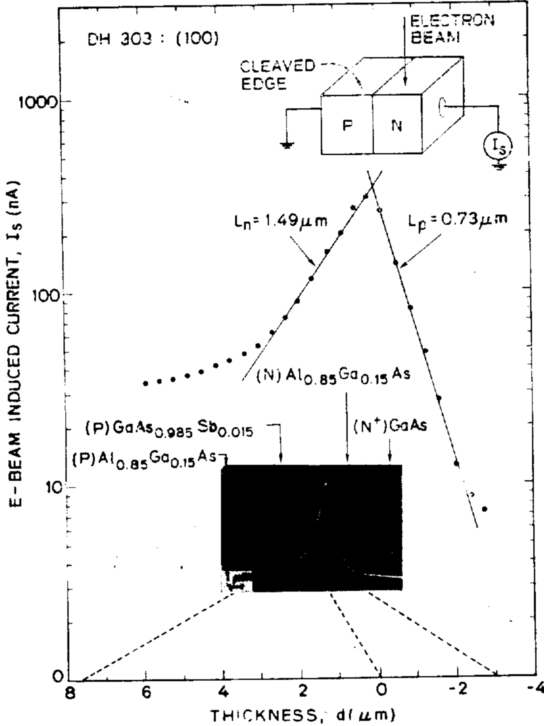

Fig. 13. Scanning electron microscope induced-current mode and semi-log plots of induced-current VS beam position.

C' real quantity

D distribution coefficient

D_n diffusion constant of electron minority carriers (cm^2/sec)

d double-heterojunction spacing (μm)

E Young-s modulus

E_f Fermi energy (eV)

E_g band-gap energy (eV)

G_s electron-hole generation rate (parirs/cm^3-sec)

I_s electron beam-induced current (nA)

L_n minoritycarrier(electron) diffusion length(μm)

L_p minority carrier (hole) diffusion length (μm)

S interface recombination velocity (cm/sec)

T_G growth temperature (°C)

W_{Al} weight of Al in melt (gm)

W_{Ga} weight of Ga in melt (gm)

W_{Sb} weight of Sb in melt (gm)

x mole fraction of AlAs in AlGaAs ternary compound.

y mole fraction of GaSb in GaAsSb ternary compound

α thermal-expansion coefficient (1/°C)

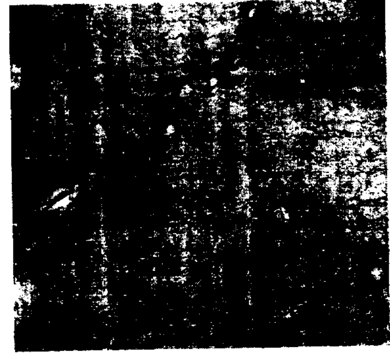

Fig. 14. Photomicrograph of surface morphology of As-Grown (100)-oriented $Al_{0.85}Ga_{0.15}As$-$GaAs_{0.985}Sb_{0.015}$ DH diode.

Δa strain-free lattice-constant difference between epitaxial layer and substrate (Å)

Δn excess minority carrier (electron) density (cm^{-3})

$\Delta\bar{n}$ average excess electron minority carrier density (cm^{-3})

$\Delta a^{\perp}$ perpendicular strained lattice-constant difference between epitaxial layer and substrate (Å)

$\Delta a^{\parallel}$ parallel strained lattice-constant difference between epitaxial layer and substrate (Å)

$\Delta\theta_B$ angular difference caused by difference of lattice spacing normal to the substrate surface (sec)

$\Delta\theta_1$ separation angle between between $K_{\alpha 1}$ peaks of substrate and epitaxial ayler (sec)

$\Delta\theta_2$ same quantitity as above, measured after rotating the crystal by 180° around the normal to the substrate surface (sec)

$\varepsilon^{\perp}$ strain perpendicular to substrate surface

$\epsilon^{\parallel}$ strain parallel to substrate surface

θ phase difference (degree)

θ_B Bragg's angle (degree)

λ wavelength (Å)

ν_{eff} effective Poisson ratio

ξ normalized interface recombination velocity

$\sigma^{\perp}$ stress perpendicular to substrate surface

$\sigma^{\parallel}$ stress parallel to substrate surface

τ_{eff} effective minority carrier lifetime (nsec)

τ_0 bulk lifetime (nsec)

ω angular frequency of a pulsed laser